Supporting Information

Boosting Interfacial Charge Transfer and Electricity Generation for Levofloxacin Elimination in Self-driven Bio-Driven Photoelectrocatalytic System

Libin Zeng[†], Xinyong Li[*†, ‡], Qidong Zhao[†], Shiying Fan[†], Mingmei Zhang[†], Zhifan Yin[†], Aicheng Chen[*‡]

†State Key Laboratory of Fine Chemicals, Key Laboratory of Industrial Ecology and Environmental Engineering (MOE), School of Environmental Science and Technology, Dalian University of Technology, Dalian 116024, China.

‡The Electrochemical Technology Centre, Department of Chemistry, University of Guelph, 50 Stone Rd E, Guelph, Ontario N1G 2W1, Canada.

Experimental details

Chemicals

MoS_2 powder (<1 μm size, 98%, Sinopharm Chemical Reagent Co., Ltd), acetonitrile (Sinopharm Chemical Reagent Co., Ltd), 1-methyl-2-pyrrolidone (NMP, Sinopharm Chemical Reagent Co., Ltd), (3-aminopropyl) trimethoxysilane (APTMS, TCI) and LEV (anhydrous, > 98.0% (HPLC), TCI).

Bulk MoS_2 exfoliation

A modified method was used to synthesis MoS_2 quantum dots (QDs).[1, 2] 1 g of MoS_2 powder was ground in a mortar and pestle with 2 mL of acetonitrile for 10 minutes, then adding an additional 2 mL and grinding for a further 10 minutes. The sample was left to dry. Meanwhile, it was added to 100 mL of NMP in a 200 mL beaker and sonicated in an ultrasonic ice bath maintaining 3 h. Then, the dispersion was ice bath ultrasonication with a sonic tip (500 W) for another 3 h. The dispersion was kept overnight, and the top supernatant was centrifuged at 6000 rpm for 60 min, to remove sediment and obtain the yellow-green MoS_2 suspension. The obtained MoS_2 QDs was kept in 4 ℃ refrigerators for further using.

Characterization

The morphology of the composite was measured by a field-emission scanning electron microscopy (FE-SEM) (Nova Nano SEM450, USA). The transmission electron microscopy (TEM) analyses were conducted by an FEI Tecnai F30 electron microscope to analyze MoS_2 QDs distribution and size. The composite electrodes were characterized by energy-dispersive X-ray spectra (EDX) (Horiba 7593H). X-ray

diffraction (XRD) using a diffractometer with Cu $K\alpha$ radiation (D/max-2400, Japan, source light at the wavelength (λ) of 0.1541 nm) was used to determine the samples of crystalline structures. The chemical compositions of electrodes were analyzed by an X-ray Photoelectron Spectroscopy (XPS) (Thermo ESCALAB 250XI, USA). The optical characterizations were tested with a UV–vis diffuse reflectance spectra (DRS) (JASCO, UV-550, Japan). Transient photovoltage spectroscopy (TPV) has been used to characterize the simples (Assembled by Jilin University, composing of monochromatic light, a lock-in amplifier (SR830-DSP), a photovoltaic cell and an operative platform). The photoluminescence spectra (PL) were probed by the Photoluminescence spectrophotometer (Hitachi FL-4500, excited at λ = 325nm) in the air at room temperature. The rate of degradation was observed in terms of the change in intensity at λ_{max} = 286.4 nm by using UV-Vis spectrophotometer (UV2300 II, Japan). The intermediates were detected using liquid chromatography/time-of-flight mass spectrometry (LC/TOF/MS) (G6224A, America Agilent Company). The electron paramagnetic resonance spectroscopy (EPR) signals of the radicals trapped were detected on a Bruker A200- 9.5/12 by using 5,5-dimethyl-1-pyrroline-N-oxide (DMPO) as a spin-trapping agent. The PEC performances of these mixed electrodes were measured using a three-electrode electrochemical workstation (CHI 760C, Shanghai Chenhua, China). Using a 16 channel data acquisition device (MPS-010602 type, China) to collect the voltage signal.

Computational methods

The energies of lowest unoccupied molecular orbital (LUMO) and highest occupied molecular orbital (HOMO) of the target contaminants LEV-H^+ molecule was calculated by density functional theory (DFT) with DMol3 module using plane-wave basis sets. The Perdew–Burke–Ernzerhof (PBE) functional of the generalized gradient approximation (GGA) was used as the exchange-correlation function.

Figure S1 showed the transmission electron microscopy (TEM) images of the as-prepared MoS_2 QDs, its size statistics were presented in Figure S1(c), the size of particles was mainly distributed between 7-10 nm through this modified method. Their high-resolution TEM was also performed in Figure S1(d), it revealed that MoS_2 QDs exposed the lattice distance of 2.54 and 2.74 Å, which were corresponded to the crystal facet of (102) and (100) (JCPDs # 37-1492), respectively.

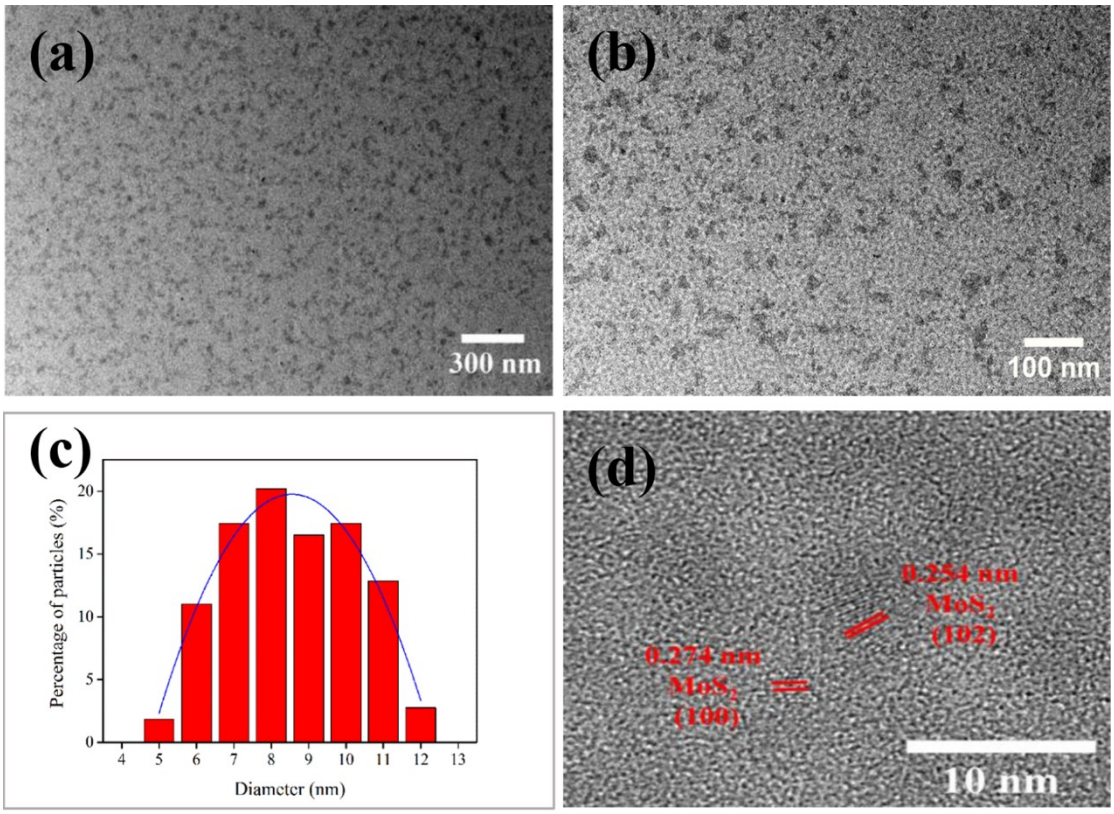

Figure S1. (a), (b) TEM images of MoS_2 quantum dots interspersed in 1-methyl-2-pyrrolidone solution; (c) the particle size distributions of MoS_2 quantum dots; (d) The HRTEM image of the MoS_2 quantum dots.

Further structural characterization was measured by the absorption spectra of the prepared MoS_2 sample (Figure S2). It exhibited the absorbance peaks at 675 and 612 nm, which are respectively ascribed to the B and A arising from the K point of the Brillouin zone [1-3]. Besides, the broad absorbance peaks at approximately 470 and 366 nm could be corresponding to the D and C of the direct transitions from the deep valence band to the conduction band[1, 4]. These finds matched well with the characteristic absorption peaks of MoS_2 nanoparticles in the solution[5]. Also, the absorption peaks in the near-UV region (λ < 300 nm) can be attributed to the excitonic features of MoS_2 quantum dots in the solution[4]. In Figure S2 (b), PL spectra indicated the strongest emission peak at 467 nm at the excitation wavelength of 380 nm. When the excitation wavelength shifted to the longer, the emission energy would move to lower, which revealed the MoS_2 QDs showed excellent quantum confinement effects.

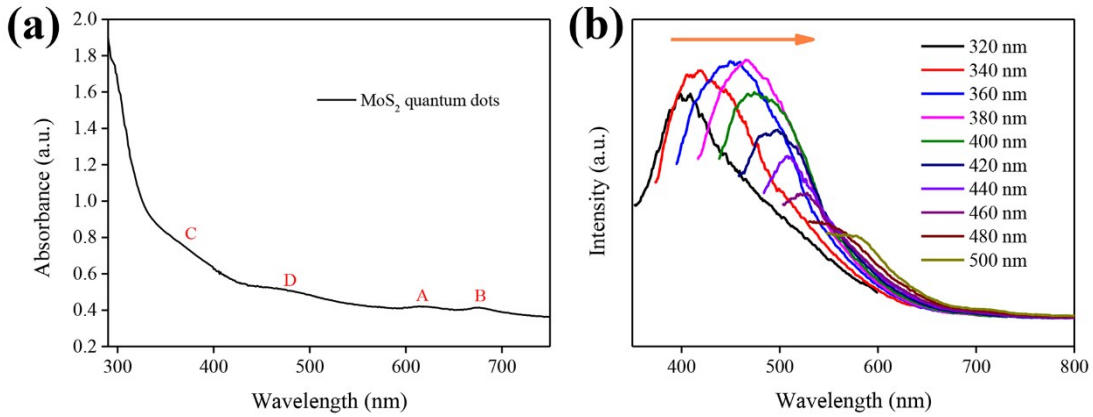

Figure S2. (a) UV-Vis absorption spectrum and (b) Photoluminescence spectra of MoS_2 QDs interspersed in NMP, with recorded at the excitation wavelength of 320-500 nm.

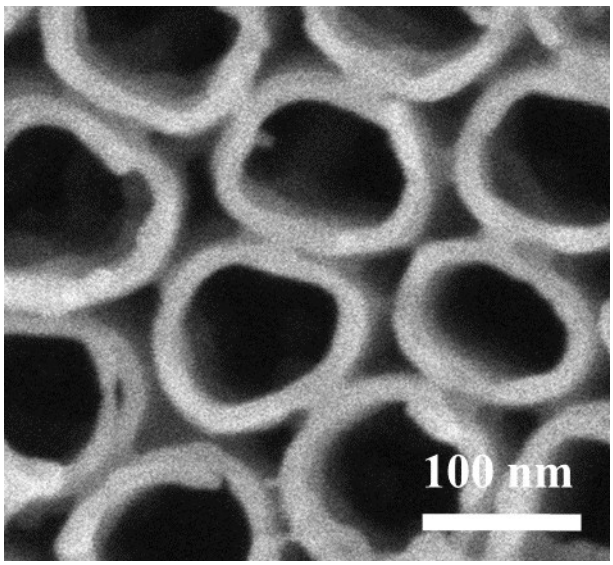

Figure S3. SEM image of pure TiO_2 NTs

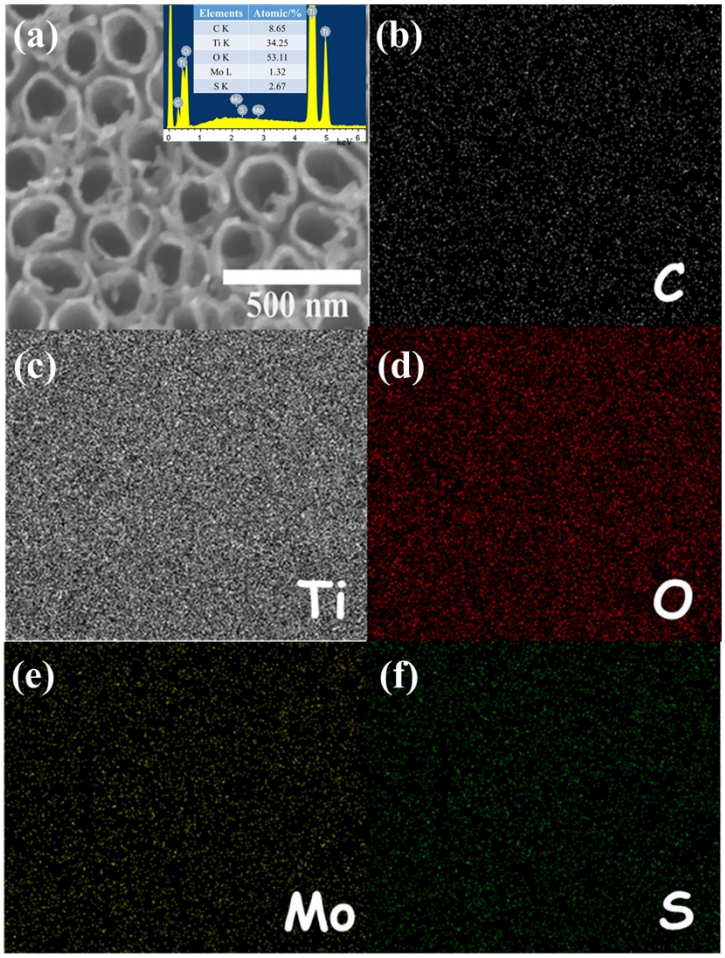

Figure S4. (a) SEM images of MoS_2 QD/TiO_2 NTAs; b–f) corresponding elemental (b): C, (c): Ti, (d): O, (e): Mo and (f) mappings of this electrode.

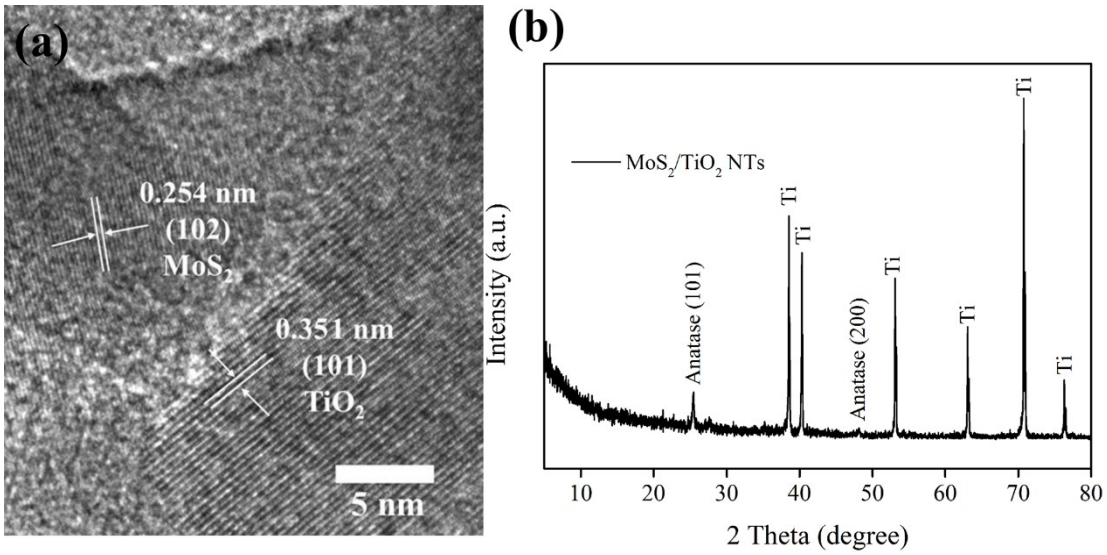

Figure S5. (a) HRTEM image and (b) XRD pattern of MoS_2 QD/TiO_2 NTAs.

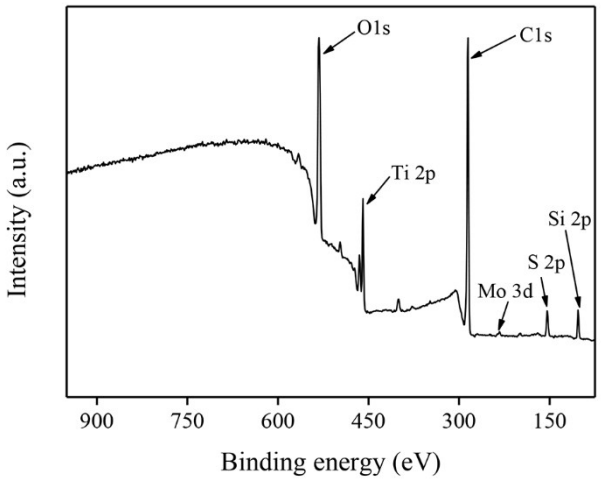

Figure S6. The wide scan X-ray photoelectron spectra (XPS) survey spectra of the composites.

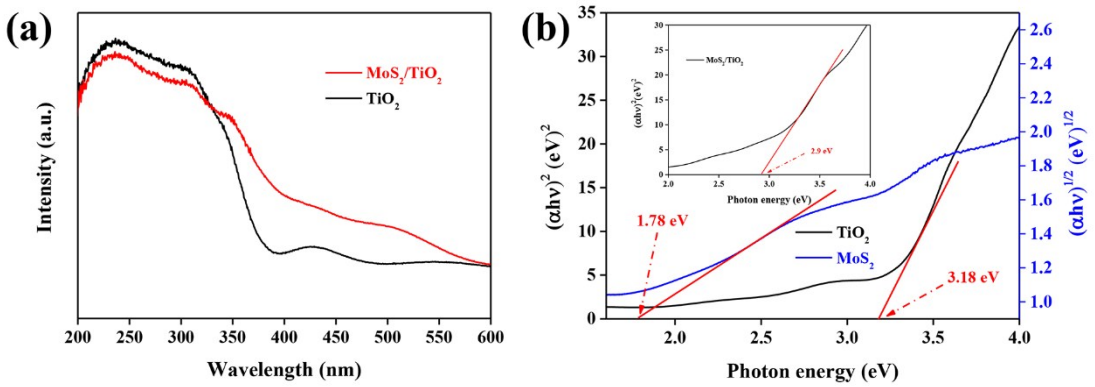

Figure S7. (a)UV−vis diffuse reflectance spectrum of MoS_2QD/TiO_2 NTAs and TiO_2 NTAs; (b) the calculated band gaps of MoS_2 and TiO_2, respectively. The inset shows the calculated bandgap of this composite.

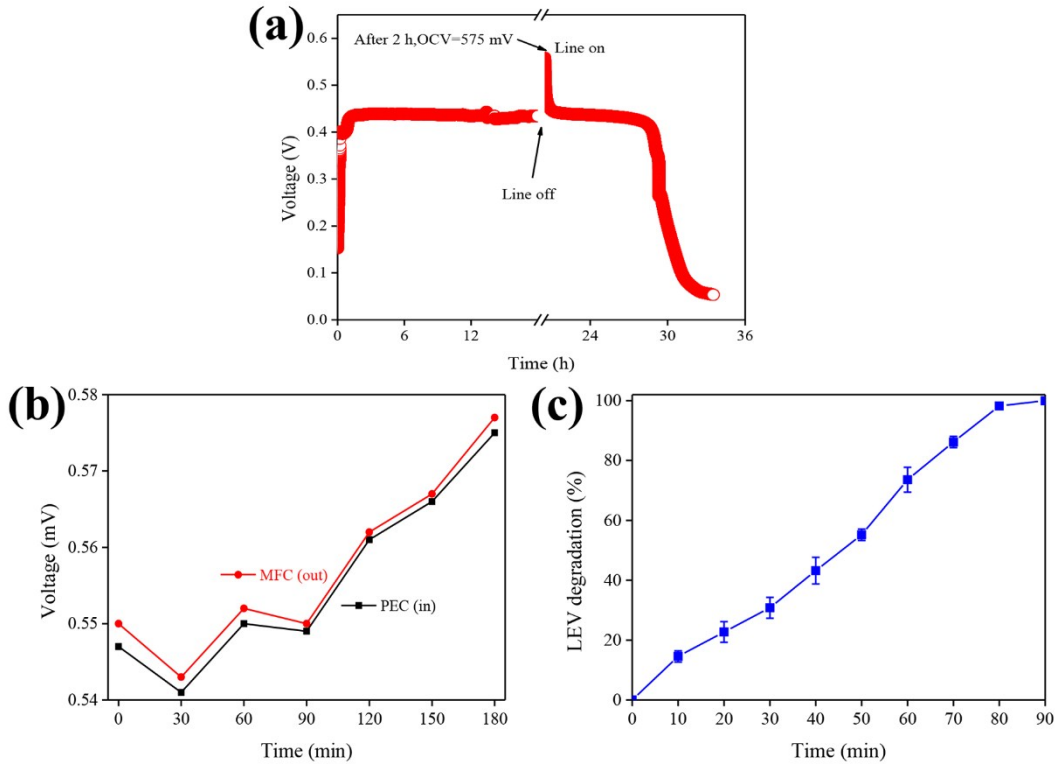

Figure S8. (a) The output voltage of SCMFC by 8 mM LEV solution under 1KΩ external resistance; (b) Plots of voltages in I-SCMFC-PEC system for degradation LEV; (c) SCMFC degradation rate of LEV by taking the sample every 10 mins, error bars refer to the standard deviation among three replicates.

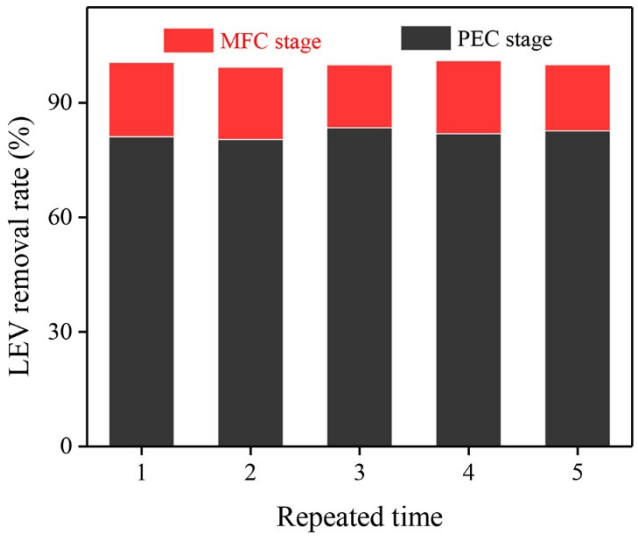

Figure S9. Typically repeated experiments for LEV degradation in S-SCMFC-PEC system.

Except for the LEV-H^+ ion, there were ten degradation products (L_1-L_{10}) (**Figure S9 (a)**), with protonated fragment ions at m/z 348.1354, 336.1354, 318.1601, 360.1554, 378.1482, 344.1313, 274.2744, 262.1133, 346.1197 and 302.1499, respectively.

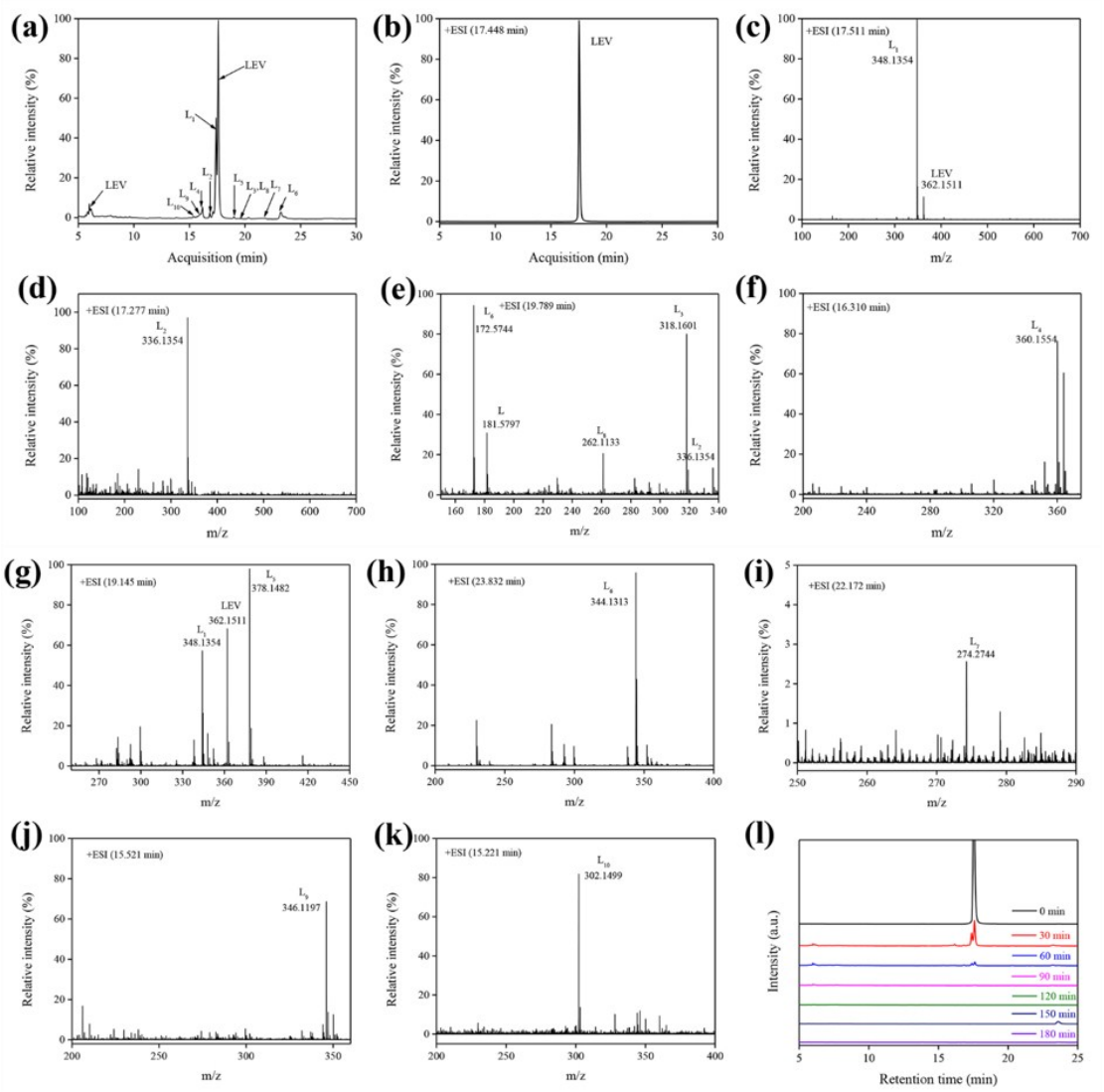

Figure S10. Accurate-Mass LC/TOF/MS chromatograms of LEV degradation for 60 min. over a MoS_2/TiO_2 electrode using the SCMFC-PEC hybrid system. (a) Peaks L1-L10: degradation products; (b-k) Different mass spectral LEV products; (l) Chromatogram of different stages of LEV degradation.

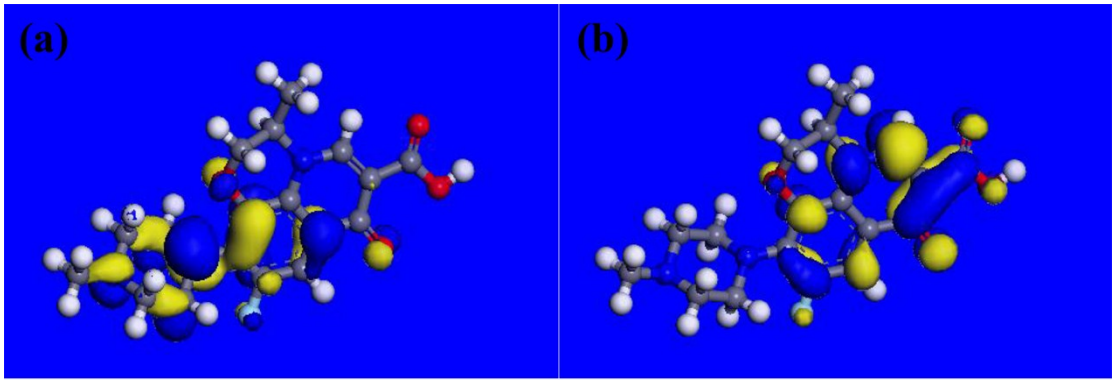

Figure S11. Calculated HOMO (a) and LUMO (b) of LEV-H^+ ion.

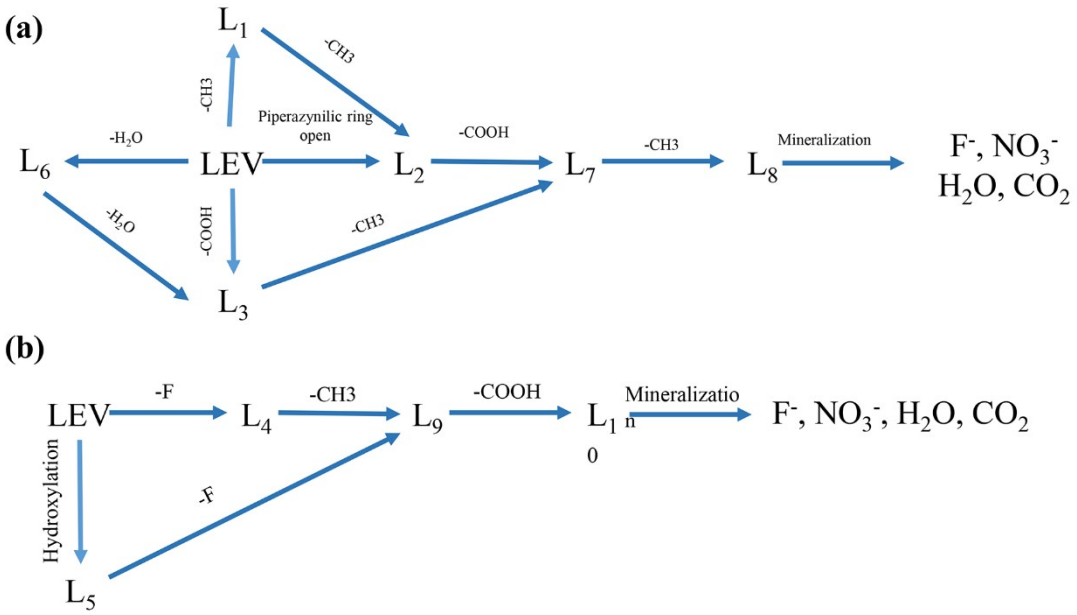

Figure S12. Two types of LEV degradation pathways.

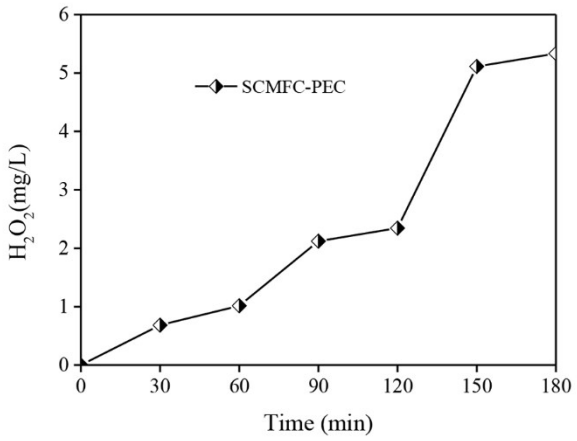

Figure S13. Yield of H_2O_2 under the SCMFC-PEC system.

References

[1] D. Gopalakrishnan, D. Damien, M.M. Shaijumon, ACS Nano 8 (2014) 5297-5303.

[2] R.M. Clark, B.J. Carey, T. Daeneke, P. Atkin, M. Bhaskaran, K. Latham, I.S. Cole, K. Kalantar-Zadeh, Nanoscale 7 (2015) 16763-16772.

[3] G. Eda, H. Yamaguchi, D. Voiry, T. Fujita, M. Chen, M. Chhowalla, Nano Lett 11 (2011) 5111-5116.

[4] V. Chikan, D. Kelley, J. Phys. Chem. B 106 (2002) 3794-3804.

[5] T. Wang, L. Liu, Z. Zhu, P. Papakonstantinou, J. Hu, H. Liu, M. Li, Energy Environ. Sci. 6 (2013) 625-633.